THE ASTROPHYSICAL JOURNAL, 434:546–551, 1994 October 20

THE 3.28 MICRON EMISSION FEATURE IN NGC 253

PAUL KALAS[1] AND C. G. WYNN-WILLIAMS
Institute for Astronomy, University of Hawaii, 2680 Woodlawn Drive, Honolulu, HI 96822
Received 1993 November 12; accepted 1994 April 27

ABSTRACT

The 3.28 μm polycyclic aromatic hydrocarbon (PAH) emission feature in the galaxy NGC 253 comes from an extended star formation region $\sim$100 pc across. The brightest mid-infrared source in the galaxy, which is displaced $\sim$45 pc from the probable nucleus, does not show the PAH feature; it may be a dust-enshrouded recent supernova.

Subject headings: galaxies: individual (NGC 253) — galaxies: ISM — galaxies nuclei

1. INTRODUCTION

NGC 253 is a nearby Sc galaxy that is of interest mainly because of its high surface brightness at most infrared wavelengths. Its bolometric infrared luminosity ($\sim 3 \times 10^{10}\ L_{\odot}$; Telesco & Harper 1980) is not in a league with the rare and distant ultraluminous galaxies found by the *IRAS* survey, but because it is close to the Sun ($\sim$3 Mpc; Tully 1988), it can be studied at a level of detail that is not possible for more distant galaxies.

The stellar disk consists of a central peak with a 20″ diameter and an extended inner disk of diameter 360″ (Scoville et al. 1985). The radio continuum emission from the central region is of nonthermal origin with many small knots superposed on an extended background (e.g., Antonucci & Ulvestad 1988). The presence of hydrogen emission lines and deep 2.3 μm CO absorption bands (Wynn-Williams et al. 1979; Rieke et al. 1980; Rieke, Lebofsky, & Walker 1988) has led to the idea that NGC 253 harbors a starburst in its central region.

The major problems in studying NGC 253 are its high inclination and the heavy, patchy extinction in its central region that hinders registration of observations made at different wavelengths; unfortunately NGC 253 does not have a single bright compact nucleus that permits unambiguous registration among optical, infrared, and radio features.

In this paper we describe infrared imagery of the central 200 pc region of NGC 253 over the wavelength range 1.6–4.8 μm. Our new observations improve on earlier infrared studies in two major ways. First, using the precise offsetting capability of the NASA Infrared Telescope Facility (IRTF), we took great care to register the images taken at different wavelengths. Second, we mapped the 3.28 μm emission feature, which is known to be strong in NGC 253 (Moorwood 1986). The 3.28 μm emission feature is widely recognized as being caused by stretch vibrations of C—H bonds present in small interstellar grains or large molecules (Sellgren 1994). The molecules are believed to be polycyclic aromatic hydrocarbons (PAHs), but the exact identification is not crucial to this work. The C—H bonds are excited when interstellar grains are heated to high, nonequilibrium temperatures by the absorption of a single UV photon (Sellgren 1984). The feature is therefore associated with the presence of these molecules in the vicinity of hot, young stars typically found in star-forming regions. Regions heated by relatively cool, evolved stars do not show the emission feature.

Maps of the spatial extent of the 3.28 μm feature may therefore indicate the size and distribution of a starburst region or the presence of an active galactic nucleus (AGN). This information is generally inaccessible at optical wavelengths due to obscuration, while radio wavelength maps mainly show the distribution of synchrotron emission whose connection with the stellar or nonstellar energy source in the galaxy is circuitous. A localized absence of the 3.28 μm feature may indicate the presence of a Seyfert nucleus or other unconventional sources of power. In this case, the microscopic grains may be destroyed by the hard photons from the AGN (Aitken & Roche 1985).

2. OBSERVATIONS

We used ProtoCAM on the NASA IRTF at Mauna Kea to obtain data under photometric conditions on 1991 September 30 and October 2. The camera was fitted with a 58 × 62 InSb detector and operated at a plate scale of 0.″3 pixel^{-1}, giving a field of view of 22″ × 20″. We used a 1.4% resolution circular variable filter (CVF) to map the PAH emission. It was set at wavelengths of 3.18, 3.28, and 3.38 μm to sample the emission feature at 3.28 μm and two adjacent continuum wavelengths. We supplemented the CVF measurements with broad-band images using standard *H*, *K*, and *M* filters at 1.6, 2.2, and 4.8 μm. Observations of standard stars indicated that the stellar images had a full width at half-maximum (FWHM) of 0.″8–1.″0.

Because of the importance of accurately registering together all our various images of NGC 253, we paid particular attention to the pointing of the telescope. Each galaxy exposure was made by first recording an image of the star SAO 166579, then offsetting the telescope to the nominal position of NGC 253. Following integration on the galaxy at the offset position, the telescope was moved back to the SAO star position and a second stellar image was recorded. The movements between the galaxy and star were made using the incremental encoders on the telescope that have a resolution of order 0.″1. We found that the centroids of the "before" and "after" stellar images usually agreed to less than 0.″7. Co-added integration times on the galaxy were typically 30 s with the broad-band filters and 200 s with the CVF filters. Background values for sky subtraction were taken from regions of the chip perpendicular and 8″–10″ away from the midplane of the galaxy.

Photometric calibration was based on the standard stars HD 201941 and HD 1160 (Elias et al. 1982). Standard image

[1] Visiting Astronomer, NASA Infrared Telescope Facility (IRTF), which is operated by the University of Hawaii under contract from the National Aeronautics and Space Administration.

processing packages in IRAF were used to reduce the data, which included flat-fielding, sky subtraction, and subsequent reregistration, and median-combining of same-wavelength frames to improve the signal-to-noise ratio.

3. RESULTS

3.1. *Maps*

Figure 1 shows logarithmic contour plots of NGC 253 at *H*, *K*, 3.28 μm, and *M*. Each map is the result of median-combining ~ 5 images. On the basis of source morphology, we identify our peak 2 with Hot Spot A of Forbes, Ward, & Depoy (1991), although we disagree in our estimate of its absolute position. Their hot spots B and C appear on our maps as distortions to the contours surrounding peak 1 rather than as distinct sources.

The stellar distribution as traced by the *K* map matches the distribution of thermal emission at *M*. We have identified four infrared peaks, which we call peaks 1, 2, 3, and 4, where peak 1 is the strongest infrared source and peak 4 the weakest. Peak 1 appears to be pointlike at *M* and in the 3.18–3.38 μm CVF images, with a FWHM perpendicular to the galaxy plane of less than 0.″8.

3.2. *Astronomy of the Infrared Sources*

Relating near-infrared, mid-infrared, and radio continuum phenomena to each other is central to understanding the physical nature of the emission sources. Note that because of the way we obtained our data, our positional results have three levels of precision. In decreasing order of precision these are

1. Relative positions of features seen at a single wavelength. In this case all the information is contained within single images of NGC 253 and avoids errors due to telescope pointing and offsetting. Errors are therefore reduced to the uncertainty in establishing the positions of the centroids of emission in each frame.

2. Registration of the maps obtained at different wavelengths. In this case we use the images of the nearby SAO star (assumed to be wavelength independent), plus the recorded telescope offsets to provide a constant reference frame by which different wavelength images may be compared. The errors in the absolute position of the SAO star are irrelevant.

3. Absolute positioning of the features, for comparison with far-infrared data and radio data. To determine the absolute positions of features in NGC 253 we need to assume a position for SAO 166579. The position we used was $\alpha = 00^h45^m7^s.45$, $\delta = -25°40'2''.55$, which is the position in the SAO Catalog corrected for proper motion from 1950 to 1991. We have compared this position to those derived from measurements in the Position and Proper Motion Star Catalog (Roser & Bastian 1991; hereafter PPMC) and the Hipparchos Input Catalog (Turon et al. 1992; hereafter HIC). All three catalogs are in

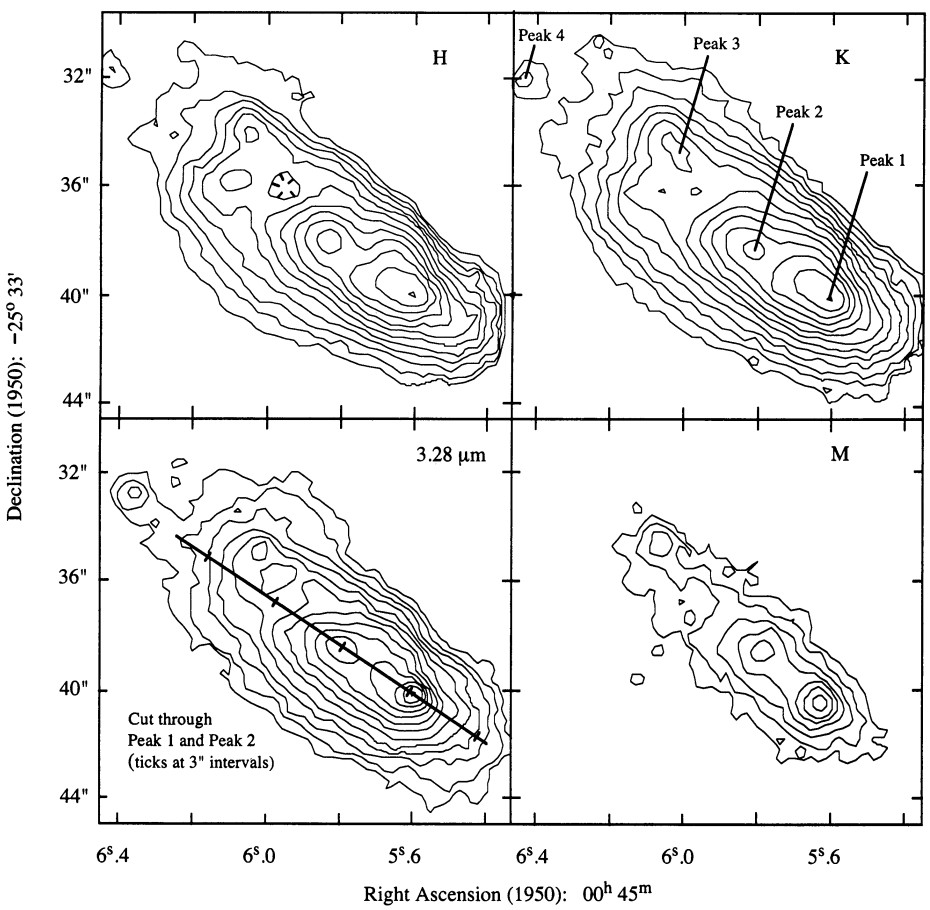

FIG. 1.—Four logarithmic contour plots of NGC 253. The contour intervals at *H*, *K*, 3.28, and *M* are 0.07, 0.075, 0.10, and 0.2 dex, respectively, with lowest contours at 0.35, 0.4, 0.8, and 1.5 mJy per square arcsecond, respectively. The 3.28 μm map includes both feature and continuum emission. In the *K* map, the four peaks are labeled, and in the 3.28 μm map the position angle and extent of the cut used for Fig. 3 is shown.

good agreement in right ascension, the listed positions after a proper motion correction not differing by more than 0^s.02 (0".3). In declination, however, the SAO position lies ~1".0 north of both the PPMC and HIC positions. Yet the PPMC and the HIC disagree with each other in that the PPMC gives a negative value for the proper motion in declination, while the HIC reports a positive value. Hence, while the right ascension for SAO 166579 appears reliable, an uncertainty of order 1".0 is associated with its declination.

The relationship between our peak positions at different wavelengths is shown in Figure 2*a*. Because we found no significant differences between the 3.18, 3.28, and 3.38 μm maps, we have averaged together positions at these wavelengths and refer to them as "L." Note that peak 4 does not have an *M*-band measurement because it was placed out of the field of view in these frames. We see in Figure 2*a* that the four positions measured for peaks 1, 2, and 3 lie within circles of radius 0".25, 0".7, and 0".4, respectively. In the cases of peaks 1 and 3, we believe that the positional discrepancies are about as good as we can expect from our observing techniques, but in the case of peak 2 there are signs of a significant wavelength-dependent discrepancy.

To investigate the possible position discrepancy in peak 2, we tried reregistering the four images using peak 1 as the reference position, rather than SAO 166579. This registration involves shifts of less than 0".3. We took the position of peak 1 to be the mean value determined at all four wavelengths. As may be seen from Figure 2*b*, this reregistration leads to a significant reduction in the position spread of peak 2 at *H*, *K*, and *L*, with a small reduction in position spread of peaks 3 and 4 at all wavelengths. However, the position of peak 2 at 4.8 μm now lies ~1".0 west of its *H*, *K*, and *L* position. We examined this discrepancy by measuring the separations and the position angles of peaks 1, 2, and 3 at *L* and *M* in individual frames, and by blinking images at different wavelengths against each other. These methods convincingly show that the discrepancy is real.

TABLE 1

POSITIONS OF NEAR-INFRARED PEAKS

λ	Source Name	Position (1950) $\alpha = 00^h45^m$	Position (1950) $\delta = -25°33'$	Reference
1.6–4.8 μm	Peak 1	05^s.615 ± 0.07	40".21 ± 1".0	1
8.5–12.5 μm	...	05^s.63 ± 0.03	40".5 ± 0".44	2
10 μm	IRS 1	05^s.63 ± 0.12	40".0 ± 1".6	3
2 cm	7	05^s.626	41".23	4
6 cm	...	05^s.625	41".24	5
1.6–3.38 μm	Peak 2	05^s.838 ± 0.07	38".49 ± 1".0	1
4.8 μm	Peak 2	05^s.765 ± 0.07	38".37 ± 1".0	1
8.5–12.5 μm	...	05^s.81 ± 0.03	38".8 ± 0".44	2
10 μm	IRS 2	05^s.74 ± 0.12	38".4 ± 1".6	3
2 cm	2	05^s.795	38".95	4
6 cm	...	05^s.794	38".99	5
1.6–4.8 μm	Peak 3	06^s.06 ± 0^s.07	34".76 ± 1".0	1
1.6–3.38 μm	Peak 4	06^s.44 ± 0^s.07	32".71 ± 1".0	1

REFERENCES.—(1) This paper; (2) Keto et al. 1992; (3) Pina et al. 1993; (4) Turner & Ho 1985; (5) Antonucci & Ulvestad 1988.

This result may be confirmed by inspection of the contour plots in Figure 1. Peaks 1, 2, and 3 lie in a relatively straight line in the *M*-band map, while at the other three wavelengths peaks 2 and 3 lie at different position angles with respect to peak 1. The method of absolute positioning indicates that while peaks 1 and 3 effectively show no change in position with wavelength, the centroid of emission of peak 2 has a different position at 1.6–3.8 μm as compared with that at 4.8 μm. Blinking different wavelength frames shows that in the *H* and *K* images a dark lane appears to be obscuring the region where peak 2 is centered in the *M* image.

We give our best estimates for the absolute positions in Table 1. We believe that our measurements for the positions of the infrared peaks relative to the star SAO 166579 are accurate to ~0".5. However, we quote errors of 1".0 to make allowance for possible errors in the published proper motion and position

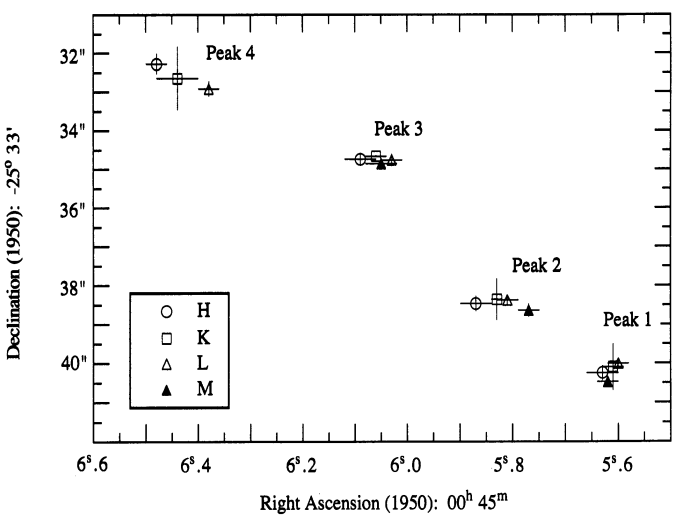

FIG. 2*a*

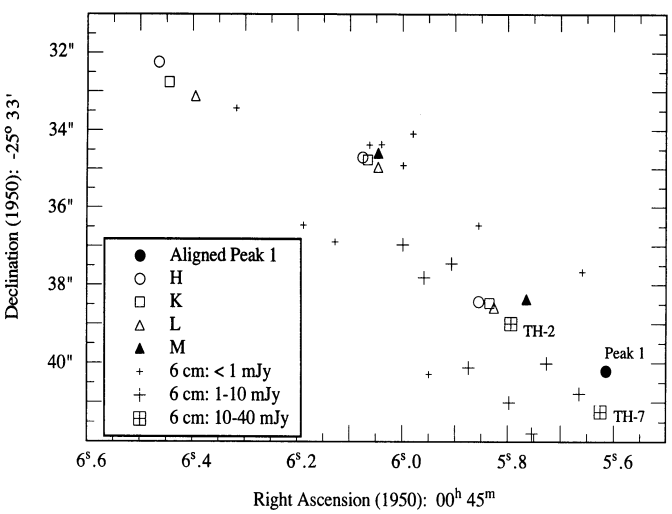

FIG. 2*b*

FIG. 2.—(*a*) The positions of peaks 1, 2, 3, and 4 are plotted on a celestial coordinate grid. The data marked "L" are the mean of the 3.18, 3.28, and 3.38 μm measurements. The *L* points result from the most number of measurements, 21, while *M* has 4, and *H* and *K* have 6 each. Errors derive from telescope pointing, offsetting, and tracking, the uncertainty in the SAO star position, and the determination of the centroid of emission on each image. The accuracy of the centroid position depends on how strong or pointlike the emission appears, and we estimate 1 $\sigma \leq 0".2$. The error bars shown represent 1 σ of the mean of the measurements at each wavelength. (*b*) The *H*, *K*, *L*, and *M* positions have been shifted to a common position for peak 1 that was determined by taking the mean value of the four positions at each wavelength of peak 1.

of SAO 166579. We have quoted our positions to more significant figures than are warranted by the absolute precision. The extra decimal place is marginally significant in discussions of the separations of the peaks, and may become useful if and when a more accurate position for SAO 166579 is subsequently published.

3.3. *Association with 10–20 Micron Sources and Radio Sources*

As may be seen in Table 1, our position for peak 1 agrees to within 0".33 with the mid-infrared positions published by Pina et al. (1992) and Keto et al. (1993). This result is consistent with the expectation that the brightest component at 4.8 μm is also the brightest point at 10–20 μm. Our position for peak 2 is also in agreement with those given by Pina et al. (1992) and Keto et al. (1993). The positions in the former paper were derived from absolute astrometry by Telesco, Dressel, & Wolstencraft (1993).

In Figure 2*b* we plot the positions of the peaks of 6 cm emission measured by Antonucci & Ulvestad (1988). The peaks have been coded according to their approximate flux densities. We see that peak 2 lies within 0".8 of radio source TH-2, the brightest of the compact radio sources in the center of NGC 253, with the radio source lying between the 1.6–3.28 μm and the 4.8 μm positions. We therefore consider it reasonable to identify TH-2 with peak 2, in agreement with Keto et al. (1993) and Pina et al. (1992), but with the reservation that peak 2 has a wavelength-dependent position.

The association of peak 1 with compact radio source TH-7 is less satisfactory because our position for peak 1 is $\sim$1" north of the radio source. The positions determined by Pina et al. and by Keto et al. echo this discrepancy. What we can say with confidence is that it is not possible to simultaneously identify TH-2 with peak 2 and TH-7 with peak 1. We are able to make this statement because we can measure the vector separations between the two infrared sources with great precision, since both peaks occur on the image frame. We find that the vector connecting the two radio sources differs from the vector connecting the two infrared sources by $\sim$0".5—about twice our estimated error for the infrared separations.

On balance, therefore, we cautiously identify peak 2 with radio source TH-2, but do not associate peak 1 with any radio source. These conclusions are in agreement with those of Pina et al. and Keto et al. We disagree with the astrometry and the identifications proposed by Forbes et al. (1991) who identify their "H-band nucleus" (our peak 1) with the radio source TH-2. We believe that their infrared image and radio map are misaligned by $\sim$3" and the radio-infrared associations that they propose are incorrect.

3.4. *3.28 Micron Feature in NGC 253*

The three images we obtained of NGC 253 at 3.18, 3.28, and 3.38 μm allow us to investigate the spatial variation of the strength of the PAH emission feature across the central region of NGC 253. We used the 3.18 and 3.38 μm images to calculate the mean continuum level and subtracted this from the 3.28 μm images to obtain a map of the strength of the 3.28 μm feature. We attempted to find a satisfactory way of presenting a two-dimensional image of the feature/continuum ratio, but found that small uncertainties in zero levels in our maps produced spurious contours in the low surface brightness regions of the ratio map that undermined its usefulness. We have therefore chosen to present our results in the form of profiles that pass through peaks 1 and 2. These are shown in Figure 3, together

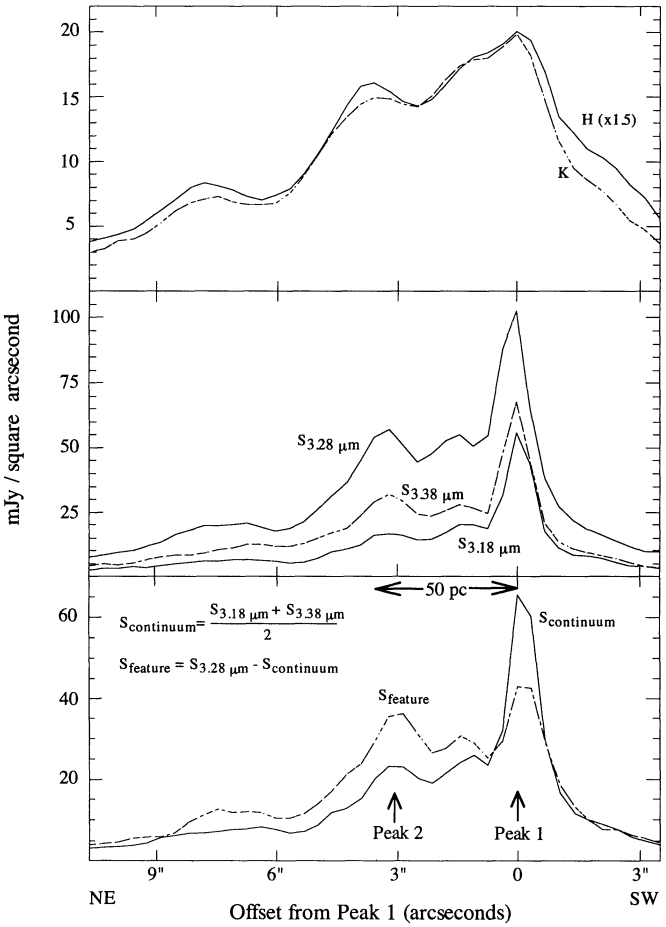

FIG. 3.—Profiles through peaks 1 and 2 of different wavelength images of NGC 253. The position angle and extent of the cut is shown in Fig. 1. In the top panel, the *H* image is scaled to match the flux from the *K* image. The plot reveals the approximate $H-K$ color variation of the galaxy, and shows a slightly bluer trend southwest of peak 1. The middle panel shows the 3.18, 3.28, and 3.38 μm images. The bottom panel demonstrates that the strength of the 3.28 μm feature is relatively uniform through the galaxy. At peak 1, however, the feature is weak relative to the continuum.

with the *H* and *K* profiles along the same line. The profiles are the mean value along a strip that is 0".7 (2 pixels) wide along the galaxy's minor axis. No smoothing has been performed along the galaxy's major axis. The extent and position angle of the cut is shown on the 3.28 μm map in Figure 1.

Two major conclusions may be drawn from the profiles. First, both the 3 μm continuum emission and the 3.28 μm PAH emission feature arise from extended regions that, to a first approximation, follow the distribution of the starlight seen at *H* and *K*. Second, the feature/continuum ratio is approximately constant over the central 80 pc of the galaxy, except at peak 1, which has a significantly lower feature/continuum ratio than the surrounding galaxy. There is some indication that the ratio is higher than average at peak 2.

We performed photometry on the three most distinct sources of emission. Peaks 1 and 2 are the strongest sources of emission in all four wavelength regions, while peak 3 is relatively weak, except in *M*, where it stands out prominently above the background. Peak 4 is the weakest and most poorly defined source of near-IR emission, and because it has large

uncertainties we exclude it from the present discussion. In Table 2 we list the flux densities obtained from 2″ diameter circular apertures centered on peaks 1, 2, and 3. The accuracy of the photometry is estimated to be ~10%. Since peak 1 appears pointlike at 3–5 μm, we have tried to separate its emission from that of the surrounding galaxy. We estimated this background contribution by taking the mean flux density from a circular ring of 0.″35 (1 pixel) width just outside the 2″ aperture. We estimate that the accuracy of the fluxes obtained from such a small aperture and with this background subtraction method is 15%–20%.

The images show that the galaxy background is generally more significant at shorter wavelengths, meaning that peak 1 is far less dominant at *H* than at *M*. In Table 2, peak 1 minus background at *H* has only 17% of the flux of peak 1 before the background subtraction, but has 67% of the flux at *M*. In the last line of Table 2, we compare the strength of the 3.28 μm feature relative to the continuum. As in Figure 3, the continuum flux is taken to be the mean of the 3.18 μm and 3.38 μm fluxes, while the feature flux is the 3.28 μm flux minus the continuum flux. At peak 1, the continuum is stronger than the 3.28 μm feature with both peak 1 and peak 1 minus background, while the background value has continuum and feature fluxes that are nearly the same. Peak 3 also has a feature/continuum ratio very near unity. At peak 2, however, the feature is stronger than the continuum. This relationship is also seen clearly in the cuts through peak 1 presented in the middle panel of Figure 3. The 3.28 μm feature is generally stronger than the continuum except at the position of peak 1. This indicates that peak 1 may be fundamentally different from peaks 2 and 3.

The bottom row of Table 2 confirms that the feature/continuum ratio is significantly lower in peak 1 than in peak 2. The background subtraction around peak 1 suffers from large uncertainties owing to the rapidly changing surface brightness in this region. We found that comparatively minor changes in the method for estimating the background flux density around peak 1 could lead to ratios anywhere between 0 and 1. In summary, we found that the feature/continuum ratio for peak 1 is significantly lower than that for the rest of the galaxy and that when background galaxy emission is subtracted the ratio may drop to 0.

3.5. *Identification of the Nucleus of NGC 253*

Although peak 1 is the brightest infrared source at all wavelengths between 1.6 and 4.8 μm, we will argue that peak 2 corresponds more closely to the true nucleus of the galaxy. As can be seen in Figure 1, peak 2 lies significantly closer to the centroid of the 2.2 μm light distribution than does peak 1. Because of the strength of the 2.3 μm CO absorption feature in NGC 253 (Rieke et al. 1980), there is little doubt that the 2.2 μm emission is produced by stars. The 2.2 μm emission is therefore probably the best guide we have in this galaxy to the distribution of mass. We have also obtained *H* and *K* maps of a much larger (~80″) field centered on the nucleus of NGC 253; these images were obtained in collaboration with Jeffrey Goldader on the UH 2.2 m telescope with a 256 × 256 NICMOS array. These images confirm that peak 2 lies closest to the centroid of near-IR emission, whereas peak 1 is displaced to the southwest of this centroid. Peak 2 also lies closer to the centroid of the radio continuum emission than does peak 1.

Several authors (e.g., Rieke et al. 1988) assume that peak 1, rather than peak 2, is the nucleus of NGC 253, and that the observed asymmetry between peak 1 and the centroid of broader, low-level emission is the result of interstellar extinction to the southwest of peak 1. However, inspection of the *H* and *K* cuts through the major axis of the galaxy in Figure 3 shows no evidence for reddening in the region southwest of peak 1. In fact, this region appears bluer than peak 1, which is not consistent with an increase of dust extinction to the southwest. Furthermore, we note that in both the 12.5 μm map of Keto et al. (1993) and the 20 μm map of Pina et al. (1992), the centroid of low-level contours still remains northeast of peak 1. As noted by Rieke & Low (1975), an unrealistically large dust column density would be required to reproduce at 10–20 μm the asymmetry observed at 2 μm. Since extinction appears to be an inconsistent explanation, and the centroid of the isophotes in the radio and in the 2–20 μm range lies closer to peak 2 than to peak 1, we suggest that peak 2 is a more plausible location for the nucleus of NGC 253.

The question remains as to whether the 1.6–3.4 μm position or the 4.8 μm position is the better estimate of the position of the nucleus. We favor the 4.8 μm position, mainly because there is less confusion caused by dust extinction at this wavelength. Support for the positioning of the true nucleus of the galaxy slightly to the west of the *K*-band peak is provided by Sams et al. (1994), who favor this position on the basis of a careful analysis of the $J-K$ colors of the region.

3.6. *The Nature of Peak 1*

The peak 1 compact infrared source has a weak 3.28 μm PAH feature relative to the other sources and is therefore probably of a different physical nature. Our observations show that it lies ~3″ (45 pc) from the nucleus of the galaxy, that it has a measured diameter of <0.″7 (10 pc), and that it does not coincide with any compact radio source. It has a low color temperature and increasingly becomes the dominant source of emission from the galaxy at wavelengths longward of 3.38 μm. A blackbody fitted through the 3.38 and 4.8 μm points would have a color temperature of 359 K, a diameter of 0.″021 (0.31

TABLE 2

FLUX DENSITY[a]

Wavelength	Peak 1	Background	Peak 1 − Background	Peak 2	Peak 3
1.65 μm, *H*	77	64	13	42	22
2.2 μm, *K*	84	63	21	55	29
3.18 μm, CVF	98	52	46	61	32
3.28 μm, CVF	222	131	91	191	75
3.38 μm, CVF	137	77	60	93	41
4.8 μm, *M*	1047	349	698	643	249
Feature/continuum	0.89	1.03	0.72	1.48	1.05

[a] 2″ diameter aperture in mJy.

pc), and a bolometric luminosity of $7 \times 10^8 L_\odot$. Extrapolation of this blackbody curve to longer wavelengths predicts an 11.7 μm flux density of 6.8 Jy, which is more than enough to account for the flux density of peak 1 as measured by Pina et al. (1992) and is more than 10% of the total density measured by *IRAS* (Soifer et al. 1989). On the other hand, the 359 K blackbody fails by a factor of 2 to account for 20 μm flux density of peak 1 measured by Pina et al., indicating that there is probably extra emission at 20 μm with a lower color temperature.

Could peak 1 be a very intense starburst? There are two reasons to doubt this hypothesis. First, the 3.28 μm emission feature in peak 1 is weak or absent. If peak 1 were powered by a cluster of newly formed OB stars, then a strong 3.28 μm emision feature should be generated at the edges of the H II regions that would surround the OB stars. Second, if peak 1 were powered by a cluster of O stars, then its radio free-free emission should be $\sim$40 mJy, based on the relationship between radio emission and infrared emission of H II regions discussed by Wynn-Williams & Becklin (1974) and by Jennings (1974). We do not have a precise limit on the radio emission from peak 1, but we note that it must be significantly less than that from source TH-7, which itself is only 10 mJy. Unless the starburst region is so small as to be self-absorbed at 6 cm (implying a diameter of less than 0".5 or 8 pc), we can conclude that the energy source in peak 1 is not a normal starburst.

Could peak 1 be an AGN? Since we have argued that peak 1 is not the nucleus of the galaxy, we cannot logically call peak 1 an AGN. Such a designation would, in any case, be premature given the absence of evidence for jets, high velocities, or compact radio emission.

What, then, is the nature of peak 1? It is an object in the size range 0.2–10 pc that radiates the power of hundreds of O stars. Its energy source either does not ionize the surrounding gas, or it has not yet had time to do so. We cautiously speculate that peak 1 might be the dust-enshrouded remnant of a supernova that exploded inside a molecular cloud one or more decades ago. We make no specific suggestions as to the physics of the explosion, except to assume that the energy of the explosion is degraded into the infrared band by a sequence of processes that ends with the heating of dust grains in an optically thick shell.

If we assume that the energy of the explosion is being converted to thermal infrared radiation at the edge of a spherical cavity in a molecular cloud, we may derive an order of magnitude timescale for the event in two ways. First, a supernova explosion of 10^{51} ergs could sustain a luminosity of $7 \times 10^8 L_\odot$ for 12 years. Second, supernova debris expanding at 10^4 km s^{-1} would excavate a 0.12 pc radius cavity in 15 years. The close agreement between these numbers is, of course, totally fortuitous, but they suggest that the timescale for the development of peak 1 should be measured in years or decades. Although $\sim$5" resolution data at 10 μm obtained over 10 years apart by Rieke & Low (1975) and Telesco et al. (1993) do not provide convincing evidence for variability, we suggest that a watch be kept for future changes in the flux density of peak 1.

4. CONCLUSIONS

From our 1.6–4.8 μm imagery of NGC 253, we draw three conclusions:

1. The 3.28 μm emission feature comes from an extended region in NGC 253 and is strongest around the position of the galaxy's nucleus.
2. The nucleus is poorly defined at near-infrared wavelengths; the closest peak to the nucleus shifts position by 1" between 3.38 and 4.8 μm.
3. The brightest source in NGC 253 lies several arcseconds away from the nucleus. We cautiously speculate that it might be a supernova embedded in a molecular cloud with an age measured in years or decades.

We thank the staff of the IRTF for assistance with the observations and Jeff Goldader for the use of images of NGC 253 obtained at the UH 2.2 m telescope. We acknowledge helpful discussions with Charlie Telesco, Eric Keto, and Bruce Sams. This work has been supported by NSF grant AST-8919563.

REFERENCES

Aitken, D. K., & Roche, P. F. 1985, MNRAS, 213, 777
Antonucci, R. R. J., & Ulvestad, J. S. 1988, ApJ, 330, L97
Elias, J. H., Frogel, J. A., Matthews, K., & Neugebauer, G. 1982, AJ, 87, 1029
Forbes, D. A., Ward, M. J., & DePoy, D. L. 1991, ApJ, 380, L63
Jennings, R. E. 1975, in H II Regions and Related Topics, ed. T. L. Wilson & D. Downes (Berlin: Springer), 137
Keto, E., Ball, R., Arens, J., Jernigan, G., Meixner, M., Skinner, C., & Graham, J. 1993, ApJ, 413, L23
Moorwood, A. F. M. 1986, A&A, 166, 4
Pina, R. K., Jones, B., Puetter, R. C., & Stein, W. A. 1992, ApJ, 401, L75
Rieke, G. H., Lebofsky, M J., Thompson, R. I., Low, F. J., & Tokunaga, A. T. 1980, ApJ, 238, 24
Rieke, G. H., Lebofsky, M. J., & Walker, C. E. 1988, ApJ, 325, 679
Rieke, G. H., & Low, F. J. 1975, ApJ, 197, 17
Roser, S., & Bastian, U. 1991, Position and Proper Motion Star Catalogue (Heidelberg: Spektrum Akademischer) (PPMC)
Sams, B. J., Genzel, R., Eckart, A., Tacconi-Garman, L., & Hofmann, R. 1994, ApJ (submitted)
Scoville, N. Z., Soifer, B. T., Neugebauer, G., Young, J. S., Matthews, K., & Yerka, J. 1985, ApJ, 289, 129
Sellgren, K. 1984, ApJ, 277, 623
———. 1994, in The Infrared Cirrus and Diffuse Interstellar Clouds, ed. R. Cutri & W. B. Latter (San Francisco: ASP), in press
Soifer, B. T., Boehmer, G., Neugebauer, G., & Sanders, D. B. 1989, AJ, 98, 766
Telesco, C. M., & Harper, D. A. 1980, ApJ, 235, 392
Telesco, C. M., Dressel, L. L., & Wolstencraft, R. D. 1993, ApJ, 414, 120
Tully, R. B. 1988, Nearby Galaxies Catalog (Cambridge Univ. Press)
Turner, J. L., & Ho, P. T. P. 1985, AJ, 299, L77
Turon, C., et al. 1992, The Hipparcos Input Catalogue (Noordwijk: ESA) (HIC)
Wynn-Williams, C. G., & Becklin, E. E. 1974, PASP, 86, 5
Wynn-Williams, C. G., Becklin, E. E., Matthews, K., & Neugebauer, G. 1979, MNRAS, 189, 163